Crystallization of Covalent Triazine Frameworks via Heterogeneous Nucleation Approach for Efficient Photocatalytic Applications

Liping Guo,[#a] Xuepeng Wang,[#a] Zhen Zhan,[a] Yueli Zhao,[a] Linjiang Chen,*[b] Tao Liu,[b] Bien Tan*[a] and Shangbin Jin*[a]

[a] School of Chemistry and Chemical Engineering, Huazhong University of Science and Technology, Luoyu Road. 1037, Wuhan, 430074, China.

[b] Department of Chemistry and Materials Innovation Factory & Leverhulme Research Centre for Functional Materials Design, University of Liverpool, 51 Oxford Street, Liverpool L73NY, UK.

KEYWORDS covalent triazine framework, nanoporous material, crystallinity, heterogeneous nucleation, photocatalysis

ABSTRACT: Crystalline covalent triazine frameworks (CTFs) have shown intriguing applications in photoelectric fields. So far, a number of synthetic strategies based on homogeneous nucleation have been reported. However, it still remains a great challenge to acquire crystalline CTFs with wide structural diversity. Here we report the synthesis of crystalline CTFs via a novel heterogeneous nucleation strategy which exhibits a wide monomer scope. The crystalline CTFs could be successfully induced and grown on the lattice planes of salt, which works as heterogeneous nucleation agent. The CTFs of different structures were successfully obtained with high degrees of crystallinity and nanosheet morphologies. These crystalline CTFs with structural diversity showed excellent activities in photocatalytic hydrogen evolution from sea water. The highest hydrogen evolution rate from "sea water" reached 791 μmol h^{-1} with a quantum yield of 12.8% under 420 nm irradiation. This work successfully demonstrated a new approach to synthesize crystalline CTFs with wide monomer scope for photoelectric applications.

INTRODUCTION

In recent years, covalent triazine frameworks (CTFs) stand out as an intriguing porous materials and have witnessed enormous research interests in gas adsorption and storage,[1-2] heterogeneous catalysis,[3-6] sensor,[7] energy storage,[8-12] photocatalysis,[13-16] and so on.[17-21] As compared to other classes of porous materials, CTFs feature robust chemical structures and heteroatom aromatic effects endowed by highly conjugated and nitrogen-rich skeletons, and thus have shown massive potentials in optoelectronic applications.[22-26] Furthermore, CTFs that combine modular synthetic versatility with ordered structures can dramatically enhance the material's optoelectronic properties, in which the efficient charge transport and separation are facilitated.[27] Thus, crystalline CTFs are highly desirable and sought with enthusiasms. Despite the tremendous progress so far, the crystalline CTFs are still limited, showing a low chemical and structural diversity compared with the more versatile covalent organic frameworks (COFs).[28-37] Therefore, it is of great importance to develop new strategies to crystallize CTFs with wide scopes of framework topologies and diverse molecular building units.[38]

Crystalline CTFs have been synthesized through several typical methods, such as molten synthesis under ionothermal conditions from aromatic nitrile[28] or amide monomers,[39] interfacial or microwave synthesis from aromatic nitrile monomers and etc.[30, 40-41] However, the harsh reaction conditions constrained the kinetic control desirable for high crystallinity and thus it generally showed a narrow scope. We have recently developed an amidine-based polycondensation reaction,[42-43] which contains a reversible imine-bond, making the kinetic control more feasible at milder conditions. The crystallization of covalent organic frameworks (COFs) has been reported to be dominated by nucleation and growth processes.[44] In order to obtain high crystallinity, it is critical to control the kinetics of the nucleation and growth processes so that the self-correction is permitted in sufficient time. In the crystallization, nucleation plays an important role for the first step.[45] There are two general nucleation approaches: homogeneous nucleation and heterogeneous nucleation. A series of crystalline CTFs has been successfully achieved by adjusting the homogeneous nucleation rate through the kinetic control of monomer concentrations.[27, 46] However, methods via heterogeneous nucleation have been underdeveloped to crystallize CTFs.

Herein, we report a new heterogeneous nucleation strategy for the synthesis of crystalline CTFs. Unlike the homogeneous nucleation approach, the external nucleation agent should be introduced in the polymerization solution. We notice that inorganic salt could be an ideal nucleation agent because they consist of crystalline lattice

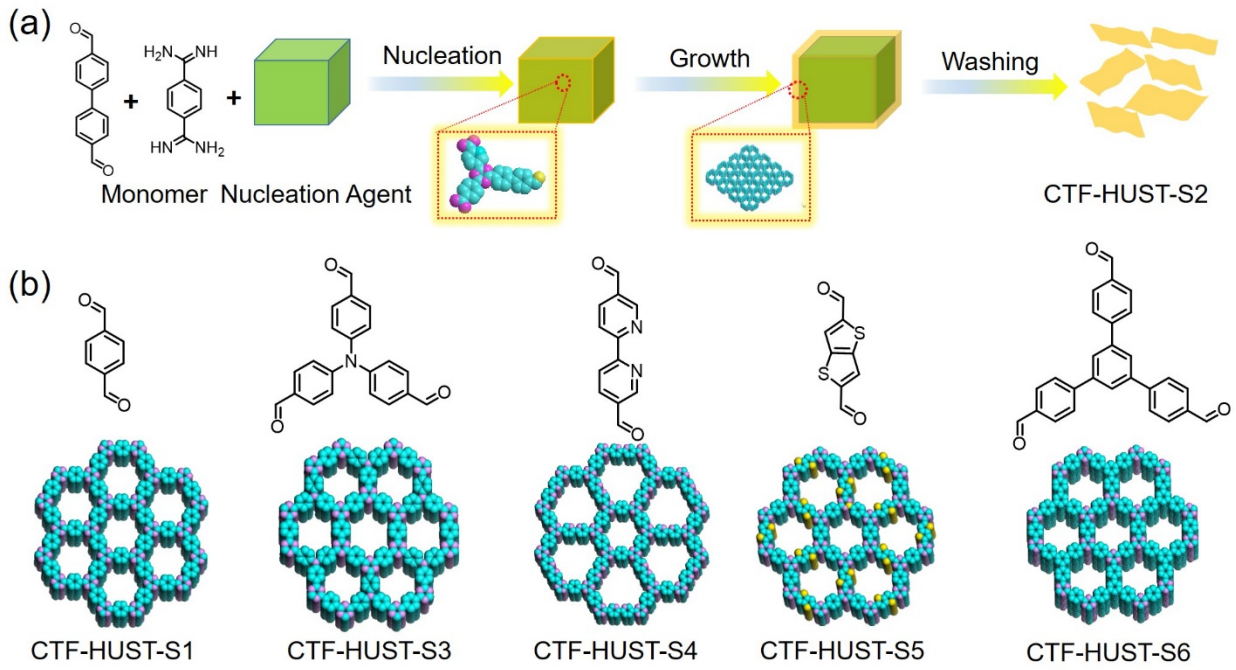

Figure 1. (a) Representative synthetic protocol of crystalline CTFs via heterogeneous nucleation. (b) Molecular structures of the aldehyde monomers and the framework structures of the corresponding crystalline CTFs.

and could be easily removed by washing with water.[47] They can also work as a physical separator to hinder the aggregation of the CTF layers and thus decrease the growth rate of the CTF crystals.[48] With the presence of inorganic salt, the growth of the crystalline CTF lattice is induced on the salt–liquid interface and the resulting CTFs tend to form nanosheet morphologies.[49] Therefore, this method possesses a distinct advantage with a wide scope of molecular building blocks. The resulting crystalline CTFs displayed excellent functional applications in photocatalytic hydrogen evolution from "sea water" for the first time. We also computationally explored the structure-property relationships of the crystalline CTFs in photocatalytic performance.

RESULTS AND DISCUSSION

The monomers were mixed with salt nucleation agent and dispersed into dimethyl sulfoxide, and then the reaction mixture was heated to initiate the polymerization. Unlike the theoretical simulation, due to the rapid precipitation of oligomers in the crystallization process, it remains a challenge to study the crystallization process of framework materials experimentally to date.[50] Here, for a better understanding of the crystallization process, we proposed a possible mechanism as shown in Figure 1. The salt has a large interface and could quickly induce the nucleation of the CTFs at the beginning of the polymerization. Then, the crystalline salt could induce the further growth of the CTF layers along the lattice planes.[51] It has been reported that the particle-particle attachment is an important step in crystallization.[52-53] Due to the presence of the large amount of nucleation agent in the solution, the CTF oligomers or large layers are spatially separated by the salts and the aggregation of them and the larger CTF crystals are hindered. Therefore, the growth rate of crystallization could be obviously slowed down. This retarded crystallization process would make the self-correction more sufficient and thus the more crystalline CTFs may be formed.

After the completion of the reaction, the nucleation agent could be easily removed by washing with water and the resulting crystalline CTFs were obtained, which are named as CTF-HUST-Sx (x = 1-6). CTF-HUST-1 to CTF-HUST-4 have been previously reported, but mainly as amorphous structures unless the kinetic controls were taken, such as controlling the monomer concentration by feeding pumps or the in-situ generation of the monomers.[43, 46, 54] We chose CTF-HUST-2 to be the benchmark model for optimizing synthetic conditions, as it has been proven relatively harder to form crystalline structures. Initially, various salt nucleation agents—including NaCl, NaBr, Na_2SO_4, KCl and LiCl—were used individually in condensation reactions of the aldehyde monomers with the amidine monomer (Supporting Information). NaCl was found to be the optimal nucleation agent, giving rise to the highest crystallinity for CTF-HUST-S2 (Figure S1). Then the amount of nucleation agent was optimized according to the PXRD peak intensity (Figure S2). The

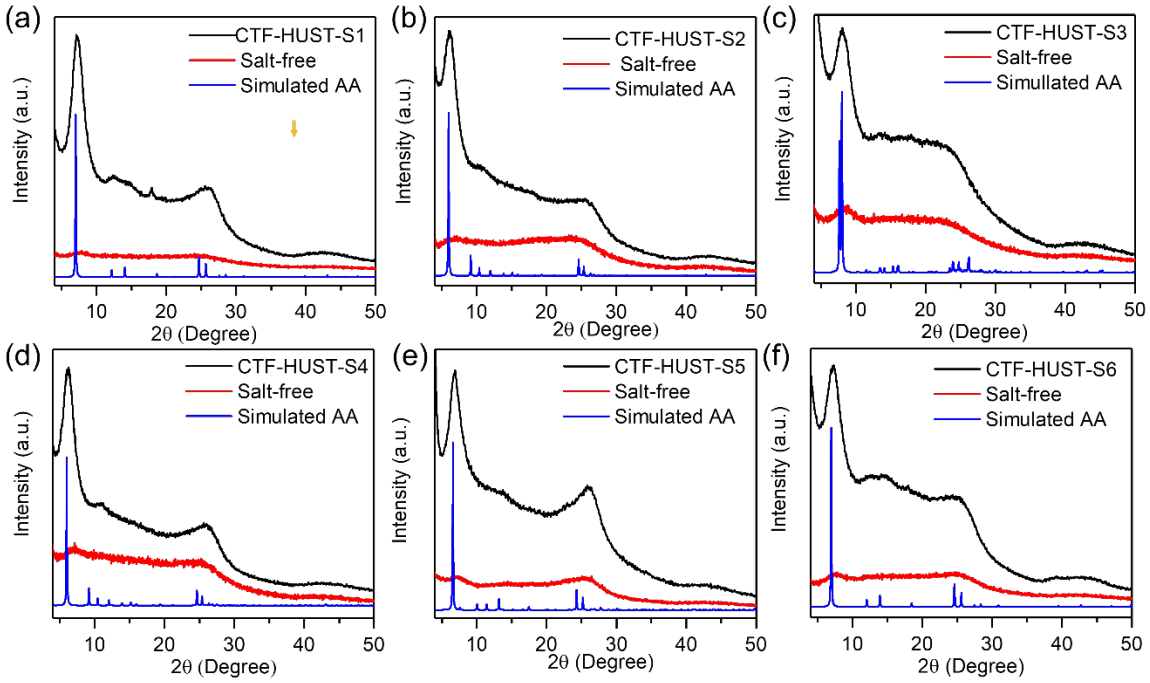

Figure 2. Experimental PXRD of the crystalline CTFs (black lines), compared with patterns obtained for the corresponding CTFs synthesized without salt-templates (red lines) and patterns simulated from structural models in the AA stacking mode (blue lines).

increased heterogeneous seeds are beneficial for crystallization with more interface for nucleation. But too much salt would affect the uniformity of the reaction system thus caused decreased crystallinity. Hereafter, we further explored the generality of this heterogeneous nucleation strategy, and successfully synthesized other examples of crystalline CTFs, i.e. CTF-HUST-S1, CTF-HUST-S3, CTF-HUST-S4, CTF-HUST-S5 and CTF-HUST-S6 (Figure 1). Among them, CTF-HUST-S3 was for the first time obtained in a crystalline form, while CTF-HUST-S5 and CTF-HUST-S6 were newly synthesized for the first time and as crystalline materials. The design of these CTFs can provide a wide structural diversity for the further applications.

As shown in Figure 2a-f, the PXRD patterns of the CTFs resulted from heterogeneous nucleation strategy exhibit strong diffraction peaks (Figure 2, black lines), confirming that the CTFs have long-range order and high periodicity in three dimensions. By contrast, the samples of the same CTFs synthesized without using external nucleation agents are mostly amorphous, with none or extremely weak PXRD signals (Figure 2, red lines). This apparent contrast illustrates that the external nucleation agent is indispensable to the formation of crystalline structures. Diffraction peaks associated with NaCl crystallites are not observed in the PXRD patterns of the CTFs (Figure S3), indicating that the salt was sufficiently removed by washing. The simulated PXRD patterns of the AA stacking mode—see Figure S4 for comparisons with the AB stacking mode—for all the CTFs agree well with the experimental PXRD data. According to the simulation results, the unit cell parameters of crystalline CTFs were $a = b = 14.53$ Å, $c = 3.61$ Å for CTF-HUST-S1, $a = b = 29.52$ Å, $c = 3.62$ Å for CTF-HUST-S2, $a = 26.61$ Å, $b = 26.64$ Å, $c = 3.79$ Å for CTF-HUST-S3, $a = b = 29.32$ Å, $c = 3.62$ Å for CTF-HUST-S4, $a = b = 26.85$ Å, $c = 3.66$ Å for CTF-HUST-S5, $a = b = 29.31$ Å, $c = 3.62$ Å for CTF-HUST-S6 (Table S5).

High resolution-transmission electron microscopy (HR-TEM) is a ubiquitous tool to reveal the crystalline structure of framework materials from a microscopic perspective. As shown in Figure 3, clear lattice structures of the crystalline CTFs are demonstrated by the HR-TEM images. Although the lattice fringes are sensitive to electron beam, some highly ordered lattices can be observed in these crystalline CTFs with robust nitrogen-rich aromatic skeletons. Furthermore, for each CTFs, the crystalline lattices can be observed in different regions, indicating the long-range ordering of the CTFs (Figure S5-Figure S10).

As shown in Figure 4, Fourier transform infrared (FT-IR) spectroscopy, solid-state CP-MAS carbon-13 nuclear magnetic resonance spectrometry (^{13}C NMR), and X-ray photoelectron spectroscopy (XPS) measurements were carried out for structural characterization of the crystalline CTFs. In line with the reported CTFs, the triazine structures were implied by the characteristic stretches at 1526 (C=N) and 1357 cm^{-1} (C-N) assigned in the FT-IR spectra (Figure 4a and Figure S11).[43] The CTF structures were further attested by solid-state ^{13}C NMR spectra,

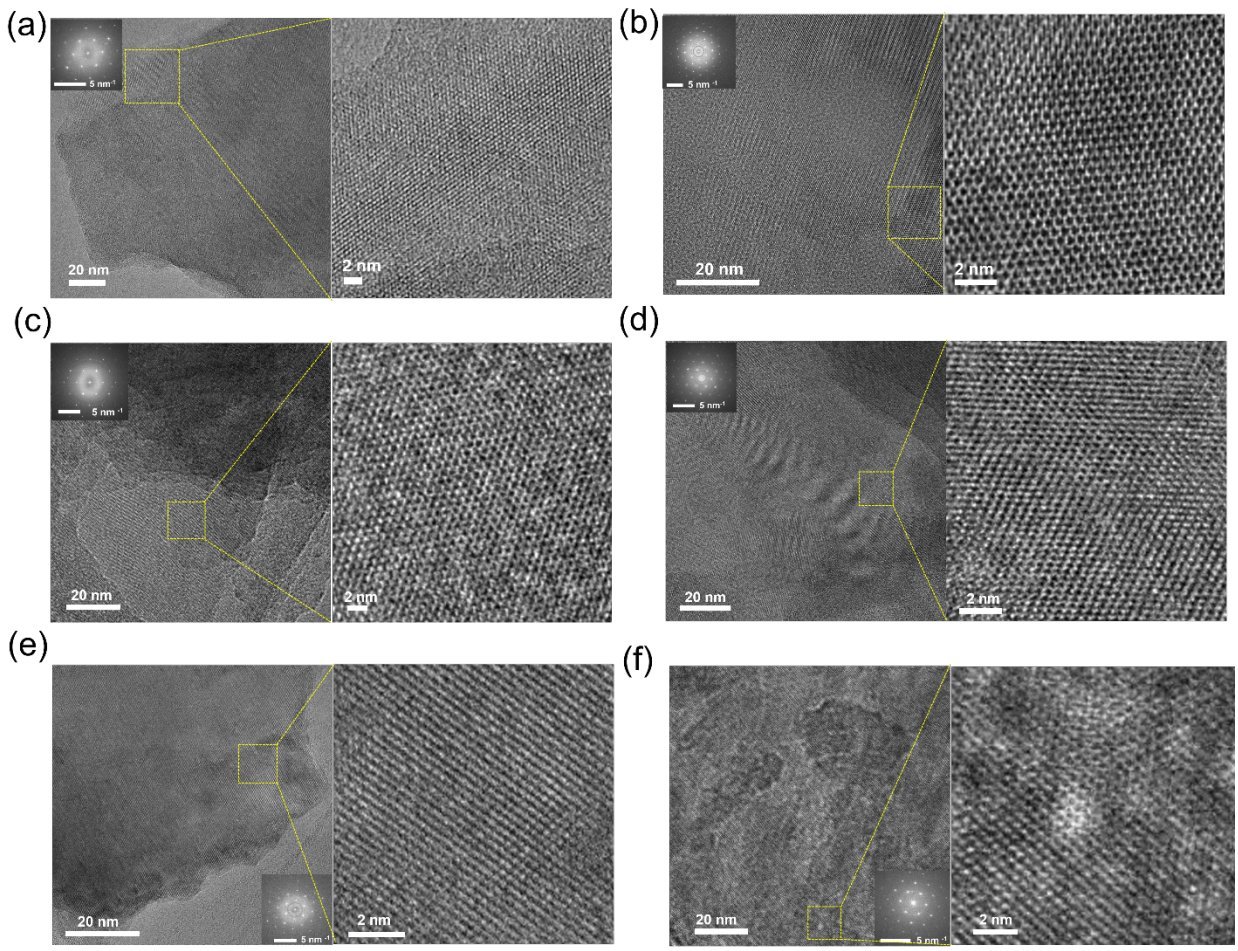

Figure 3. HR-TEM images of the crystalline CTFs, with scale bars of 20 nm and 2 nm (insets: FFT images): (a) CTF-HUST-S1, (b) CTF-HUST-S2, (c) CTF- HUST-S3, (d) CTF- HUST-S4, (e) CTF- HUST-S5, (f) CTF- HUST-S6.

which describe the characteristic chemical shifts of triazine carbon atoms at 170 ppm and other carbon atoms derived from their unique structures (Figure 4b). Moreover, XPS reveals the elements and bonding types in the crystalline CTFs (Figure S12). As shown in Figure 4c, the high-resolution N 1s surveys of the crystalline CTFs display a peak at 398.8 eV, derived from C=N-C of the triazine moiety, which can only be deconvoluted into a single peak. To compare the difference in structure between CTF samples synthesized with or without a salt nucleation agent, we measured the XPS of CTF-HUST-2 synthesized under salt-free condition (Figure S13): the XPS peak at 398.8 eV was deconvoluted into two contributing peaks withthe binding energies of 398.7 eV (corresponding to C=N-C) and 399.5 eV. The latter may be assigned to defect sites, in the form of C-N-C, in the CTFs synthesized under salt-free condition, demonstrating that the addition of heterogeneous nucleation agent promotes well-defined structures, less prone to defective triazine units. The XPS surveys also show that there was no residual sodium ion in the CTFs (Figure S14), consistent with the ICP results, confirming that the salts were completely removed. The elemental compositions of the crystalline CTFs are close to the theoretical values according to elemental analysis results (Table S1). Notably, the elemental contents of the crystalline CTFs synthesized in this strategy show smaller deviations from the ideal structures as compared to their amorphous counterparts (Table S2). As depicted in the thermogravimetric analysis curves in Figure S15, the crystalline CTFs did not markedly lose weight until 630°C under nitrogen atmosphere. The crystalline CTFs show higher thermal stabilities than their amorphous counterparts (Figure S16), which may be attributed to their more ordered and less defective structures.

Nitrogen adsorption-desorption isotherm measurements at 77 K were conducted to probe the porosity of CTF-HUST-S1 to S6 (Figure 5), with their porosity characteristics summarized in Table S3. The Brunauer–Emmett–Teller (BET) surface areas of CTF-HUST-S1 to S6 are 618, 623, 715, 470, 454, and 800 $m^2 g^{-1}$, respectively. These surface area values are comparable with previously reported crystalline CTFs.[30, 32, 40] The experimental pore diameters of the CTFs, as indicated by the corresponding

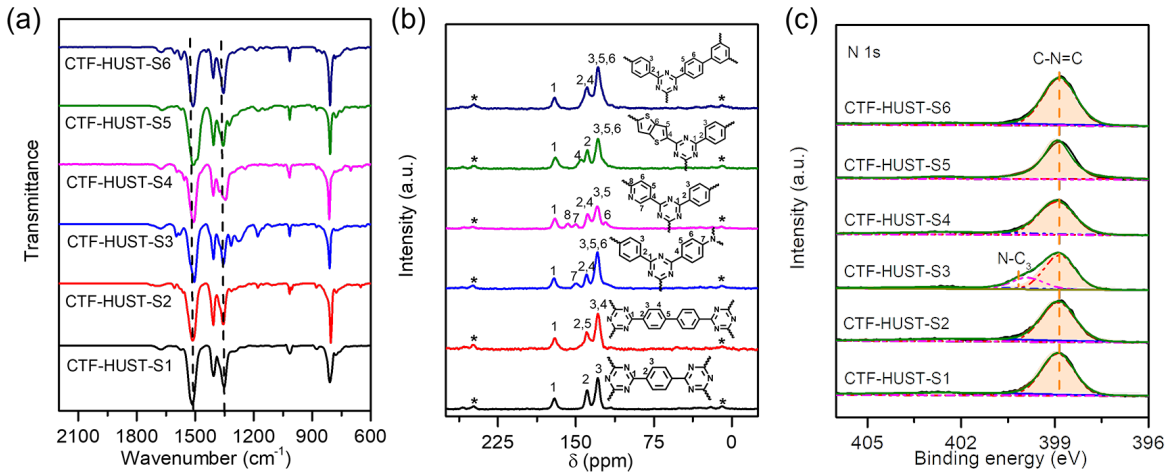

Figure 4. FT-IR spectra (a), solid-state ^{13}C NMR spectra (b) and high-resolution XPS N 1s spectra (c) for CTF-HUST-S1 to CTF-HUST-S6.

pore size distribution derived from the N_2 isotherm (insets in Figure 5), are in the range from 1.2 nm to 1.8 nm, in agreement with the theoretical models.

Benefited from the crystal surfaces of the salt nucleation agent, the CTFs were found to form nanosheet morphologies (Figure S17-S18).[55] The crystalline CTFs disperse well in water (Figures S18-S19) and ethanol (Figure S20), exhibiting pronounced Tyndall phenomenon. Thin nanosheet morphologies are clearly demonstrated for the crystalline CTFs by the TEM images after dispersion in water as shown in Figure S18: the thin layers are found in large domains with a lateral size of 1 μm to 5 μm. These thin layered morphologies may also be a good benefit for various applications such as photocatalysis. The newly synthesized, crystalline CTFs show good absorption in the visible light region (Figure S21), suggesting potentials to enable visible-light-driven photocatalysis. As an active hydrogen evolution photocatalyst, the CTF must not only absorb the visible light efficiently over a wide range, but also need to transport photo-generated electron–hole pairs, or excitons, and free charges.[56-57] We experimentally determined the HOMO/LUMO energy levels of CTF-HUST-S1 to S6, confirming that they could, at least, in principle drive photocatalytic hydrogen evolution (Figure S22-S24). The different molecular building blocks used to construct these CTFs afforded well-adjustable photoelectric properties (Figure S25-S27)

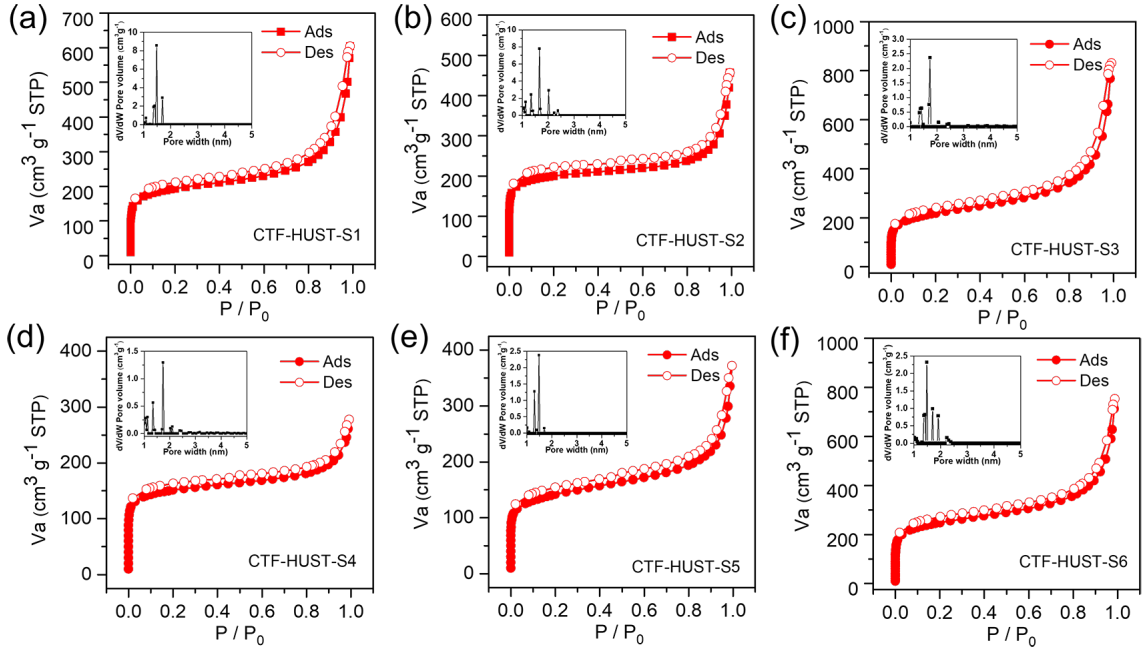

Figure 5. Nitrogen adsorption and desorption isotherms of the crystalline CTFs at 77 K (insets: the corresponding pore size distribution using a cylinder-pore model): (a) CTF-HUST-S1, (b) CTF-HUST-S2, (c) CTF-HUST-S3, (d) CTF-HUST-S4, (e) CTF-HUST-S5, (f) CTF-HUST-S6.

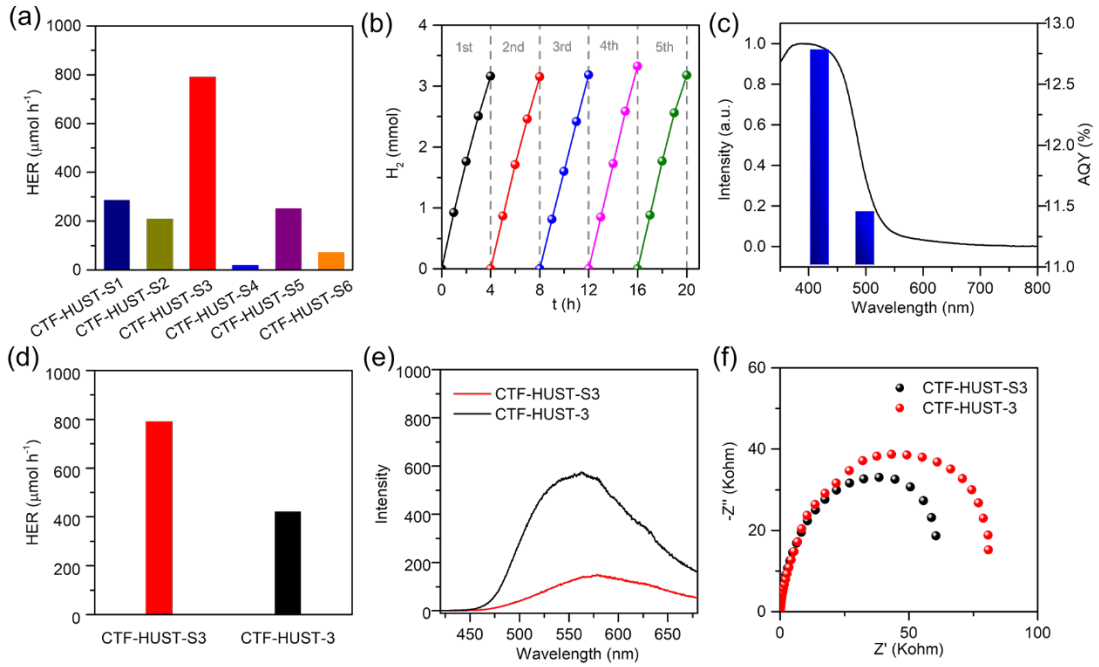

Figure 6. (a) Hydrogen evolution rates (HER) of CTFs over four hours under visible light irradiation from "sea water". (b) Recyclability performance of CTF-HUST-S3 for photocatalytic hydrogen production from "sea water". (c) UV–vis absorption spectrum and apparent quantum yields (AQY) at two different incident light wavelengths (420 nm and 500 nm) for CTF-HUST-S3. (d) Comparison of the HERs between CTF-HUST-S3 and CTF-HUST-3 in "sea water". (e) Steady-state photoluminescence spectra of CTF-HUST-S3 and CTF-HUST-3. (f) Electrochemical impedance spectroscopy (EIS) Nyquist plots of CTF-HUST-S3 and CTF-HUST-3.

Sea water is the most abundant water source on earth; thus, it is highly desirable to produce hydrogen directly from sea water.[58] Photocatalytic hydrogen evolution from pure water has been intensively studied. Yet, few efforts have been launched on using porous organic solids as photocatalysts for hydrogen evolution from sea water. As a proof of concept, 3 wt% NaCl solution was used as mimicked "sea water".[59] As shown in Figure 6, the CTFs display high photocatalytic hydrogen evolution activities (Figure 6a and Figure S28-S29) as well as good stabilities (Figure 6b). CTF-HUST-S3 gave a hydrogen evolution rate (HER) of 791 μmol h^{-1} and an apparent quantum yield (AQY) of 12.8% at 420 nm and AQY of 11.4% at 500 nm (Figure 6c). Furthermore, when the real sea water source was used, CTF-HUST-S3 still exhibited the stable photocatalytic performance (812 μmol h^{-1}) (Figure S30-S31). The photocatalytic hydrogen evolution performance is the highest in crystalline CTFs[27, 42, 60] and is also comparable to most photocatalytically active crystalline COFs.[61-63]

The photocatalytic hydrogen evolution performance of a CTF may be influenced by a plethora of the material's photoelectric properties, as well as mesoscale factors. Among the crystalline CTFs studied here, CTF-HUST-S5 shows the best light harvesting ability (Figure S21) and the smallest electron impedance (Figure S25), positively contributing to its relatively high hydrogen production. The most active photocatalyst CTF-HUST-S3 (Figure 6a, Figure S28) gives the highest photocurrent response (Figure S26) and the lowest photoluminescence intensity (Figure S27), indicating that CTF-HUST-S3 is most conducive among the series, corroborating the computational results that rank it as the best for charge separation and redistribution. Furthermore, the photoluminescence intensity of CTF-HUST-S3 is decreased as compared to its amorphous counterpart CTF-HUST-3, indicating that charge recombination is restrained (Figure 6e). Likewise, the lower electrical impedance (Figure 6f) and the higher photocurrent (Figure S26) of CTF-HUST-S3, compared to CTF-HUST-3, suggest that the increased long-range ordering improves the charge separation and transport in CTF-HUST-S3. Consequently, the crystalline CTF-HUST-S3 (791 μmol h^{-1}) outperforms its amorphous counterpart (421 μmol h^{-1}) in hydrogen production, clearly demonstrating the importance of optimizing the crystallinity of CTFs for enhanced functional properties.

To further probe the molecular-level mechanisms and structure–property relationships for the CTF photocatalysts synthesized here, we computationally studied these systems using both periodic calculations on the CTF crystal structures and cluster calculations on representative molecular fragments of the CTFs (Figure S32-S37). To work as an effective photocatalyst, the CTF is required to thermodynamically drive the reduction of protons and

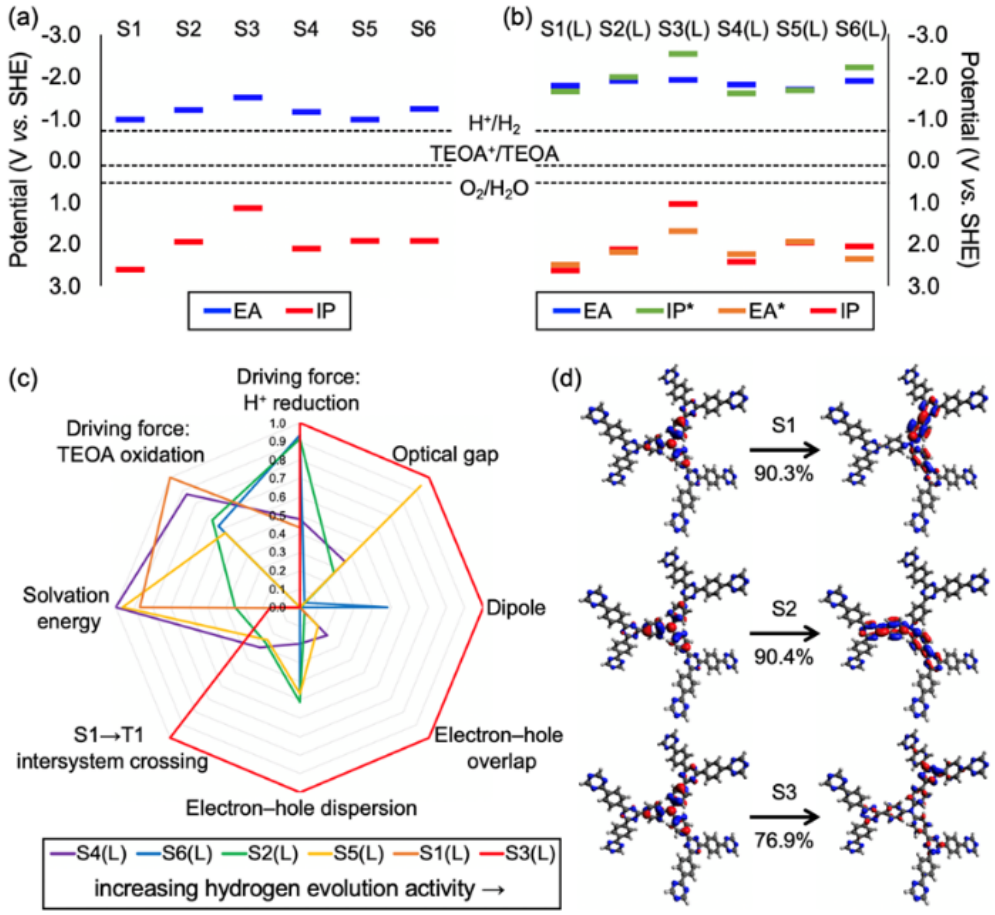

Figure 7. Electronic structure calculations provide insights into the photocatalytic water splitting activities of the CTFs. (a) Periodic DFT (HSE06) predicted IP and EA of the CTFs with respect to a common vacuum level. (b) (TD-)wB97XD predicted IP, EA, IP* and EA* vertical potentials of representative molecular fragments CTF-HUST-S1(L) to S6(L) of CTF-HUST-S1 to S6, respectively. (c) Radar plot comparing the representative molecular fragments for a series of key electronic and excited-state properties potentially influencing the hydrogen evolution activity. For each metric, the values from the different CTF fragments were proportionally normalized to be between zero and one, indicating the least and the most desirable, respectively; large absolute values are desirable for driving forces, dipole, electron–hole dispersion and solvation energy, whereas small absolute values are desirable for optical gap, electron–hole overlap and energy gap between the S1 and T1 excited states. (d) Natural transition orbitals (NTOs) for the dominant component transition of each of the first three excited state (S1–S3) of CTF-HUST-S3(L), with the corresponding contribution from the NTO pair labelled below the arrow indicating the transition.

the oxidation of, in this study, the sacrificial agent TEOA. That is, the CTF's electron affinity (EA) or exciton ionization potential (IP*) and the CTF's ionization potential (IP) or its exciton electron affinity (EA*) must bracket the proton reduction and the TEOA oxidation potentials.[61]

Periodic DFT calculations of the CTF-HUST-S1 to S6 crystal structures yielded HSE06 band gaps (Figure S38) in good agreement with the experimental optical gaps. The IP and EA of each CTF crystal structure are approximated as the Kohn–Sham valence-band-maximum and conduction-band-minimum positions of the HSE06 band structure, aligned to a common vacuum level (see details in Supporting Information Section 18). Our results show that CTF-HUST-S1 to S6 are all thermodynamically able to reduce protons and oxidize TEOA, in line with experiments (Figure 7a). CTF-HUST-S3 is shown to have the largest driving force for proton reduction—the energy difference between CTF's EA and the proton reduction potential—among the series, corroborating its highest hydrogen evolution rate.

Cluster DFT (wB97XD) calculations on representative molecular fragments of the CTFs agree with our periodic results: CTF-HUST-S1 to S6 should all have substantial thermodynamic driving forces for proton reduction and TEOA oxidation (Figure 7b). Moreover, the exciton potentials (IP* and EA*) are all confirmed to be thermodynamically able to drive exciton dissociation at the photocatalyst–solution interface, thereby participating the corresponding half reactions. This is important because exciton dissociation in the bulk material can be difficult for polymeric materials.

It is well-established that the actual hydrogen evolution activity can be influenced by a host of factors, from atomic/molecular structures up to macroscopic materials

morphologies and reaction processes. Here, we compare CTF-HUST-S1(L) to S6(L) for a range of key electronic and excited-state properties (Figure 7c): thermodynamic driving forces for the half reactions, light absorption (optical gap, E_{gap}), excited-state charge distribution (change in dipole moment between S1 and S0, ΔD; electron–hole dispersion, Δσ) and separation (electron – hole overlap, Sr), wettability (solvation energy, E_{sol}) and energy gap between the first singlet state and triplet states ($\Delta E_{S1\rightarrow T1}$); see Table S6 for details. The most photocatalytically active CTF-HUST-S3(L) is ranked at the top of the list for six out of the eight performance metrics: the largest driving force for proton reduction, strongest light absorption, largest spatial separation between the excited-state electron and hole densities, and highest probability of intersystem crossing (Figure 7c, Table S6). None of the other five CTFs is ranked the highest among the series in multiple properties. To characterize the specific transition associated with each of the S1–S3 excited states, natural transition orbitals (NTOs) were generated and are shown in Figure 7d and Figures S32–S37. For all the three excited states (S1–S3) of CTF-HUST-S3(L), there is a dominant NTO transition from the triphenylamine unit to its neighbouring triazine units (Figure 7d), with a sizable electron–hole distance (D in Table S7), showing that there are appreciable charge redistributions between the different units of the backbone upon electronic excitation. By contrast, NTO analyses of the other five CTF fragments show that all the excitations probed are heavily localized on the individual building units of the CTFs (Figures S32–S37 and Table S7).

CONCLUSIONS

In summary, we successfully developed a heterogeneous nucleation strategy to construct crystalline CTFs with a wide monomer scope. It provides a convenient synthetic route to create CTFs with structural diversity for functional applications. The photocatalytic hydrogen evolution performance was significantly enhanced due to the structural diversity and the improved crystallinity of the material. It is conceivable that the CTFs may well attain better performances as they get closer to their ordered, ideal structures. Our synthetic strategy demonstrated here may open up a promising avenue to combine crystallinity and chemical diversity in CTFs for improved synthetic tunability and versatility, and ultimately enhanced functional properties.

ASSOCIATED CONTENT

SUPPORTING INFORMATION.

This material is available free of charge via the Internet at http://pubs.acs.org.

This file is comprised of the experiment details and characterization results of CTF-HUST-SX, including the XRD patterns of CTF-HUST-S2 with different salts, simulated PXRD results, HR-TEM images, FT-IR spectra, XPS results, morphology, structural and contents analysis, photocatalysis performance and computational details.

AUTHOR INFORMATION

Corresponding Author

* jinsb@hust.edu.cn
* bien.tan@hust.edu.cn
* lchen@liverpool.ac.uk

Author Contributions

#These two authors contributed equally.

ACKNOWLEDGMENT

S.J. acknowledge the National Natural Science Foundation of China (Grant No. 21875078). L.C. and T.L. gratefully acknowledge funding from the UK's Engineering and Physical Sciences Research Council (EPSRC) (EP/N004884/1) and the Leverhulme Trust via the Leverhulme Research Centre for Functional Materials Design. We thank Xue Wang (University of Liverpool) for assistance with structural modelling and Wen Luo (Xiamen University) for providing real sea water. We also express our thanks to the Analysis and Testing Center of Huazhong University of Science and Technology for their supporting in the characterizations.

REFERENCES

(1) Tuci, G.; Pilaski, M.; Ba, H.; Rossin, A.; Luconi, L.; Caporali, S.; Pham-Huu, C.; Palkovits, R.; Giambastiani, G. Unraveling Surface Basicity and Bulk Morphology Relationship on Covalent Triazine Frameworks with Unique Catalytic and Gas Adsorption Properties. *Adv. Funct. Mater.* **2017**, *27*, 1605672.

(2) Zhao, Y.; Yao, K. X.; Teng, B.; Zhang, T.; Han, Y. A Perfluorinated Covalent Triazine-Based Framework for Highly Selective and Water-Tolerant CO_2 Capture. *Energy Environ. Sci.* **2013**, *6*, 3684-3692.

(3) Gunasekar, G. H.; Park, K.; Ganesan, V.; Lee, K.; Kim, N.-K.; Jung, K.-D.; Yoon, S. A Covalent Triazine Framework, Functionalized with Ir/N-Heterocyclic Carbene Sites, for the Efficient Hydrogenation of CO_2 to Formate. *Chem. Mater.* **2017**, *29*, 6740-6748.

(4) Chan-Thaw, C. E.; Villa, A.; Katekomol, P.; Su, D.; Thomas, A.; Prati, L. Covalent Triazine Framework as Catalytic Support for Liquid Phase Reaction. *Nano Lett.* **2010**, *10,* 537-541.

(5) Jena, H. S.; Krishnaraj, C.; Schmidt, J.; Leus, K.; Van Hecke, K.; Van Der Voort, P. Effect of Building Block Transformation in Covalent Triazine-Based Frameworks for Enhanced CO_2 Uptake and Metal-Free Heterogeneous Catalysis. *Chem. Eur. J.* **2020**, *26*, 1548-1557.

(6) Zhu, G.; Shi, S.; Zhao, L.; Liu, M.; Gao, J.; Xu, J. Catalytic Activation of Carbon–Hydrogen Bonds in Lignin Linkages over Strong-Base-Modified Covalent Triazine Frameworks for Lignin Oxidative Cleavage. *ACS Catal.* **2020**, *10*, 7526-7534.

(7) Bhunia, A.; Esquivel, D.; Dey, S.; Fernandez-Teran, R.; Goto, Y.; Inagaki, S.; Van Der Voort, P.; Janiak, C. A Photoluminescent Covalent Triazine Framework: CO2 Adsorption, Light-Driven Hydrogen Evolution and Sensing of Nitroaromatics. *J. Mater. Chem. A* **2016,** *4*, 13450-13457.

(8) Li, Y.; Zheng, S.; Liu, X.; Li, P.; Sun, L.; Yang, R.; Wang, S.; Wu, Z.-S.; Bao, X.; Deng, W.-Q. Conductive Microporous Covalent Triazine-Based Framework for High-Performance Electrochemical Capacitive Energy Storage. *Angew. Chem. Int. Ed.* **2018,** *58*, 7992-7996.

(9) Hao, L.; Ning, J.; Luo, B.; Wang, B.; Zhang, Y.; Tang, Z.; Yang, J.; Thomas, A.; Zhi, L. Structural Evolution of 2D Microporous Covalent Triazine-Based Framework toward the Study of High-Performance Supercapacitors. *J. Am. Chem. Soc.* **2015,** *137*, 219-225.

(10) Zhou, T.; Zhao, Y.; Choi, J. W.; Coskun, A. Lithium-Salt Mediated Synthesis of a Covalent Triazine Framework for Highly Stable Lithium Metal Batteries. *Angew. Chem. Int. Ed.* **2019**, *58*, 16795-16799.

(11) Je, S. H.; Kim, H. J.; Kim, J.; Choi, J. W.; Coskun, A. Perfluoroaryl-Elemental Sulfur SNAr Chemistry in Covalent Triazine Frameworks with High Sulfur Contents for Lithium-Sulfur Batteries. *Adv. Funct. Mater.* **2017**, *27*, 1703947.

(12) Buyukcakir, O.; Ryu, J.; Joo, S. H.; Kang, J.; Yuksel, R.; Lee, J.; Jiang, Y.; Choi, S.; Lee, S. H.; Kwak, S. K.; Park, S.; Ruoff, R. S. Lithium Accommodation in a Redox - Active Covalent Triazine Framework for High Areal Capacity and Fast - Charging Lithium - Ion Batteries. *Adv. Funct. Mater.* **2020**, *30*, 2003761.

(13) Wang, N.; Cheng, G.; Guo, L.; Tan, B.; Jin, S. Hollow Covalent Triazine Frameworks with Variable Shell Thickness and Morphology. *Adv. Funct. Mater.* **2019,** *29*, 1904781.

(14) Meier, C. B.; Clowes, R.; Berardo, E.; Jelfs, K. E.; Zwijnenburg, M. A.; Sprick, R. S.; Cooper, A. I. Structurally Diverse Covalent Triazine-Based Framework Materials for Photocatalytic Hydrogen Evolution from Water. *Chem. Mater.* **2019**, *31*, 8830-8838.

(15) Huang, W.; Byun, J.; Rorich, I.; Ramanan, C.; Blom, P. W. M.; Lu, H.; Wang, D.; Caire da Silva, L.; Li, R.; Wang, L.; Landfester, K.; Zhang, K. A. I. Asymmetric Covalent Triazine Framework for Enhanced Visible-Light Photoredox Catalysis via Energy Transfer Cascade. *Angew. Chem. Int. Ed.* **2018,** *57*, 8316-8320.

(16) Huang, W.; Huber, N.; Jiang, S.; Landfester, K.; Zhang, K. A. I. Covalent Triazine Framework Nanoparticles via Size-Controllable Confinement Synthesis for Enhanced Visible Light Photoredox Catalysis. *Angew. Chem. Int. Ed.* **2020**, 10.1002/anie.202007358.

(17) Hao, L.; Ning, J.; Zhi, L.; Hao, L.; Zhang, S.; Ning, J.; Zhang, S.; Liu, R.; Zhang, G. Bottom-Up Construction of Triazine-Based Frameworks as Metal-Free Electrocatalysts for Oxygen Reduction Reaction. *Adv. Mater.* **2015**, *27*, 3190-3195.

(18) Kamiya, K.; Hashimoto, K.; Nakanishi, S.; Kamai, R. Platinum-Modified Covalent Triazine Frameworks Hybridized with Carbon Nanoparticles as Methanol-Tolerant Oxygen Reduction Electrocatalysts. *Nat. Commun.* **2014,** *5*, 5040.

(19) Kamai, R.; Kamiya, K.; Hashimoto, K.; Nakanishi, S. Oxygen-Tolerant Electrodes with Platinum-Loaded Covalent Triazine Frameworks for the Hydrogen Oxidation Reaction. *Angew. Chem. Int. Ed.* **2016,** *55,* 13184-13188.

(20) Krishnaraj, C.; Jena, H. S.; Leus, K.; Van Der Voort, P. Covalent Triazine Frameworks – A Sustainable Perspective. *Green Chem.* **2020**, *22*, 1038-1071.

(21) Lu, C.; Yang, J.; Wei, S.; Bi, S.; Xia, Y.; Chen, M.; Hou, Y.; Qiu, M.; Yuan, C.; Su, Y.; Zhang, F.; Liang, H.; Zhuang, X. Atomic Ni Anchored Covalent Triazine Framework as High Efficient Electrocatalyst for Carbon Dioxide Conversion. *Adv. Funct. Mater.* **2019**, *29*, 1806884.

(22) Li, J.; Liu, P.; Tang, Y.; Huang, H.; Cui, H.; Mei, D.; Zhong, C. Single-Atom Pt–N_3 Sites on the Stable Covalent Triazine Framework Nanosheets for Photocatalytic N2 Fixation. *ACS Catal.* **2020,** *10*, 2431-2442.

(23) Kuecken, S.; Acharjya, A.; Zhi, L.; Schwarze, M.; Schomaecker, R.; Thomas, A. Fast Tuning of Covalent Triazine Frameworks for Photocatalytic Hydrogen Evolution. *Chem. Commun.* **2017,** *53*, 5854-5857.

(24) Schwinghammer, K.; Hug, S.; Mesch, M. B.; Senker, J.; Lotsch, B. V. Phenyl-Triazine Oligomers for Light-Driven Hydrogen Evolution. *Energy Environ. Sci.* **2015**, *8*, 3345-3353.

(25) Li, L.; Fang, W.; Zhang, P.; Bi, J.; He, Y.; Wang, J.; Su, W. Sulfur-Doped Covalent Triazine-Based Frameworks for Enhanced Photocatalytic Hydrogen Evolution from Water under Visible Light. *J. Mater. Chem. A* **2016**, *4*, 12402-12406.

(26) Yu, W.; Gu, S.; Fu, Y.; Xiong, S.; Pan, C.; Liu, Y.; Yu, G. Carbazole-Decorated Covalent Triazine Frameworks: Novel Nonmetal Catalysts for Carbon Dioxide Fixation and Oxygen Reduction Reaction. *J. Catal.* **2018**, *362*, 1-9.

(27) Liu, M.; Huang, Q.; Wang, S.; Li, Z.; Li, B.; Jin, S.; Tan, B. Crystalline Covalent Triazine Frameworks by In Situ Oxidation of Alcohols to Aldehyde Monomers. *Angew. Chem. Int. Ed.* **2018**, *57*, 11968-11972.

(28) Kuhn, P.; Antonietti, M.; Thomas, A. Porous, Covalent Triazine-Based Frameworks Prepared by Ionothermal Synthesis. *Angew. Chem. Int. Ed.* **2008**, *47*, 3450-3453.

(29) Bojdys, M. J.; Jeromenok, J.; Thomas, A.; Antonietti, M. Rational Extension of the Family of Layered, Covalent, Triazine-Based Frameworks with Regular Porosity. *Adv. Mater.* **2010**, *22*, 2202-2205.

(30) Ren, S.; Bojdys, M. J.; Dawson, R.; Laybourn, A.; Khimyak, Y. Z.; Adams, D. J.; Cooper, A. I. Porous, Fluorescent, Covalent Triazine-Based Frameworks Via Room-Temperature and Microwave-Assisted Synthesis. *Adv. Mater.* **2012**, *24*, 2357-2361.

(31) Fu, Y.; Wang, Z.; Li, S.; He, X.; Pan, C.; Yan, J.; Yu, G. Functionalized Covalent Triazine Frameworks for Effective CO2 and SO2 Removal. *ACS Appl. Mater. Interfaces* **2018**, *10*, 36002-36009.

(32) Yang, Z.; Chen, H.; Wang, S.; Guo, W.; Wang, T.; Suo, X.; Jiang, D. E.; Zhu, X.; Popovs, I.; Dai, S. Transformation Strategy for Highly Crystalline Covalent Triazine Frameworks: From Staggered AB to Eclipsed AA Stacking. *J. Am. Chem. Soc.* **2020**, *142*, 6856-6860.

(33) Côté, A. P.; Benin, A. I.; Ockwig, N. W.; O'Keeffe, M.; Matzger, A. J.; Yaghi, O. M. Porous, Crystalline, Covalent Organic Frameworks. *Science* **2005**, *310*, 1166-1170.

(34) Jin, E.; Asada, M.; Xu, Q.; Dalapati, S.; Addicoat, M. A.; Brady, M. A.; Xu, H.; Nakamura, T.; Heine, T.; Chen, Q.; Jiang, D. Two-Dimensional sp2 Carbon–Conjugated Covalent Organic Frameworks. *Science* **2017**, *357*, 673-676.

(35) Ma, T.; Kapustin, E. A.; Yin, S. X.; Liang, L.; Zhou, Z.; Niu, J.; Li, L.-H.; Wang, Y.; Su, J.; Li, J. Single-Crystal X-Ray Diffraction Structures of Covalent Organic Frameworks. *Science* **2018**, *361*, 48-52.

(36) Biswal, B. P.; Chandra, S.; Kandambeth, S.; Lukose, B.; Heine, T.; Banerjee, R. Mechanochemical Synthesis of Chemically Stable Isoreticular Covalent Organic Frameworks. *J. Am. Chem. Soc.* **2013**, *135*, 5328-5331.

(37) Li, Y.; Chen, W.; Xing, G.; Jiang, D.; Chen, L. New Synthetic Strategies Toward Covalent Organic Frameworks. *Chem. Soc. Rev.* **2020,** *49*, 2852-2868.

(38) Liu, M.; Guo, L.; Jin, S.; Tan, B. Covalent Triazine Frameworks: Synthesis and Applications. *J. Mater. Chem. A* **2019,** *7*, 5153-5172.

(39) Yu, S. Y.; Mahmood, J.; Noh, H. J.; Seo, J. M.; Jung, S. M.; Shin, S. H.; Im, Y. K.; Jeon, I. Y.; Baek, J. B. Direct Synthesis of a Covalent Triazine-Based Framework from Aromatic Amides. *Angew. Chem. Int. Ed.* **2018**, *57*, 8438-8442.

(40) Liu, J.; Zan, W.; Li, K.; Yang, Y.; Bu, F.; Xu, Y. Solution Synthesis of Semiconducting Two-Dimensional Polymer via Trimerization of Carbonitrile. *J. Am. Chem. Soc.* 2017, *139*, 11666-11669.

(41) Liu, J.; Lyu, P.; Zhang, Y.; Nachtigall, P.; Xu, Y. New Layered Triazine Framework/Exfoliated 2D Polymer with Superior Sodium-Storage Properties. *Adv. Mater.* **2018**, *30*, 1705401.

(42) Zhang, S.; Cheng, G.; Guo, L.; Wang, N.; Tan, B.; Jin, S. Strong Base Assisted Synthesis of Crystalline Covalent Triazine Framework with High Hydrophilicity via Benzylamine Monomer for Photocatalytic Water Splitting. *Angew. Chem. Int. Ed.* **2020**, *59*, 6007-6014.

(43) Wang, K.; Yang, L. M.; Wang, X.; Guo, L.; Cheng, G.; Zhang, C.; Jin, S.; Tan, B.; Cooper, A. Covalent Triazine Frameworks via a Low - Temperature Polycondensation Approach. *Angew. Chem. Int. Ed.* **2017**, *56*, 14149-14153.

(44) Li, H.; Evans, A. M.; Castano, I.; Strauss, M. J.; Dichtel, W. R.; Bredas, J. L. Nucleation-Elongation Dynamics of Two-Dimensional Covalent Organic Frameworks. *J. Am. Chem. Soc.* **2020**, *142*, 1367-1374.

(45) Evans, A. M.; Parent, L. R.; Flanders, N. C.; Bisbey, R. P.; Vitaku, E.; Kirschner, M. S.; Schaller, R. D.; Chen, L. X.; Gianneschi, N. C.; Dichtel, W. R. Seeded Growth of Single-Crystal Two-Dimensional Covalent Organic Frameworks. *Science* **2018**, *361*, 52-57.

(46) Liu, M.; Jiang, K.; Ding, X.; Wang, S.; Zhang, C.; Liu, J.; Zhan, Z.; Cheng, G.; Li, B.; Chen, H.; Jin, S.; Tan, B. Controlling Monomer Feeding Rate to Achieve Highly Crystalline Covalent Triazine Frameworks. *Adv. Mater.* **2019**, *31,* 1807865.

(47) Yu, H.; Yang, X.; Xiao, X.; Chen, M.; Zhang, Q.; Huang, L.; Wu, J.; Li, T.; Chen, S.; Song, L.; Gu, L.; Xia, B. Y.; Feng, G.; Li, J.; Zhou, J. Atmospheric-Pressure Synthesis of 2D Nitrogen-Rich Tungsten Nitride. *Adv. Mater.* **2018**, *30*, 1805655.

(48) Yuan, Y. C.; Sun, B.; Cao, A. M.; Wang, D.; Wan, L. J. Heterogeneous Nucleation and Growth of Highly Crystalline Imine-Linked Covalent Organic Frameworks. *Chem. Commun.* **2018**, *54,* 5976-5979.

(49) Xiao, X.; Song, H.; Lin, S.; Zhou, Y.; Zhan, X.; Hu, Z.; Zhang, Q.; Sun, J.; Yang, B.; Li, T.; Jiao, L.; Zhou, J.; Tang, J.; Gogotsi, Y. Scalable Salt-Templated Synthesis of Two-Dimensional Transition Metal Oxides. *Nat. Commun.* **2016**, *7,* 11296.

(50) Li, H.; Chavez, A. D.; Li, H.; Li, H.; Dichtel, W. R.; Bredas, J. L. Nucleation and Growth of Covalent Organic Frameworks from Solution: The Example of COF-5. *J. Am. Chem. Soc.* **2017**, *139*, 16310-16318.

(51) Xiao, X.; Yu, H.; Jin, H.; Wu, M.; Fang, Y.; Sun, J.; Hu, Z.; Li, T.; Wu, J.; Huang, L.; Gogotsi, Y.; Zhou, J. Salt-Templated Synthesis of 2D Metallic MoN and Other Nitrides. *ACS Nano* **2017,** *11*, 2180-2186.

(52) Mirabello, G.; Ianiro, A.; Bomans, P. H. H.; Yoda, T.; Arakaki, A.; Friedrich, H.; De With, G.; Sommerdijk, N. Crystallization by Particle Attachment is A Colloidal Assembly Process. *Nat. Mater.* **2020**, *19*, 391-396.

(53) Wang, Y.; Li, L.; Liang, H.; Xing, Y.; Yan, L.; Dai, P.; Gu, X.; Zhao, G.; Zhao, X. Superstructure of a Metal-Organic Framework Derived from Microdroplet Flow Reaction: An Intermediate State of Crystallization by Particle Attachment. *ACS Nano* **2019**, *13,* 2901-2912.

(54) Liu, M.; Wang, X.; Liu, J.; Wang, K.; Jin, S.; Tan, B. Palladium as a Superior Cocatalyst to Platinum for Hydrogen Evolution Using Covalent Triazine Frameworks as a Support. *ACS Appl. Mater. Interfaces* **2020**, *12*, 12774-12782.

(55) Shi, X.; Ma, D.; Xu, F.; Zhang, Z.; Wang, Y. Table-Salt Enabled Interface-Confined Synthesis of Covalent Organic Framework (COF) Nanosheets. *Chem. Sci.* **2020**, *11*, 989-996.

(56) Huang, W.; He, Q.; Hu, Y.; Li, Y. Molecular Heterostructures of Covalent Triazine Frameworks for Enhanced Photocatalytic Hydrogen Production. *Angew. Chem. Int. Ed.* **2019,** *58*, 8676-8680.

(57) Hu, Y.; Huang, W.; Wang, H.; He, Q.; Zhou, Y.; Yang, P.; Li, Y.; Li, Y. Metal-Free Photocatalytic Hydrogenation Using Covalent Triazine Polymers. *Angew. Chem. Int. Ed.* **2020**, *59*, 14378-14382.

(58) Yang, X.; Hu, Z.; Yin, Q.; Shu, C.; Jiang, X. F.; Zhang, J.; Wang, X.; Jiang, J. X.; Huang, F.; Cao, Y. Water - Soluble Conjugated Molecule for Solar - Driven Hydrogen Evolution from Salt Water. *Adv. Funct. Mater.* **2019**, *29,* 1808156.

(59) Zhang, G.; Lin, L.; Li, G.; Zhang, Y.; Savateev, A.; Wang, X.; Antonietti, M. Ionothermal Synthesis of Triazine-Heptazine Based Co-Frameworks with Apparent Quantum Yields of 60 % at 420 nm for Solar Hydrogen Production from "Sea Water". *Angew. Chem. Int. Ed.* **2018,** *57,*9372-9376.

(60) Xie, J.; Shevlin, S. A.; Ruan, Q.; Moniz, S. J. A.; Liu, Y.; Liu, X.; Li, Y.; Lau, C. C.; Guo, Z. X.; Tang, J. Efficient Visible Light-Driven Water Oxidation and Proton Reduction by an Ordered Covalent Triazine-Based Framework. *Energy Environ. Sci.* **2018**, *11,* 1617-1624.

(61) Wang, X.; Chen, L.; Chong, S. Y.; Little, M. A.; Wu, Y.; Zhu, W. H.; Clowes, R.; Yan, Y.; Zwijnenburg, M. A.; Sprick, R. S.; Cooper, A. I. Sulfone-Containing Covalent Organic Frameworks for Photocatalytic Hydrogen Evolution from Water. *Nat. Chem.* **2018,** *10*, 1180-1189.

(62) Stegbauer, L.; Zech, S.; Savasci, G.; Banerjee, T.; Podjaski, F.; Schwinghammer, K.; Ochsenfeld, C.; Lotsch, B. V. Tailor-Made Photoconductive Pyrene-Based Covalent Organic Frameworks for Visible-Light Driven Hydrogen Generation. *Adv. Eenrgy Mater.* **2018**, *8*, 1703278.

(63) Vyas, V. S.; Haase, F.; Stegbauer, L.; Savasci, G.; Podjaski, F.; Ochsenfeld, C.; Lotsch, B. V. A Tunable Azine Covalent Organic Framework Platform for Visible Light-Induced Hydrogen Generation. *Nat. Commun.* **2015**, *6*, 8508.

(64) Köhler, A.; Beljonne, D. The Singlet–Triplet Exchange Energy in Conjugated Polymers. *Adv. Funct. Mater.* **2004**, *14*, 11-18.

SYNOPSIS TOC

We report a novel heterogeneous nucleation approach to synthesize crystalline CTFs with wide monomer scope. The lattice plane of nucleation agent provides the place for CTFs growing and crystallizing and also prevent the aggregation of the CTF layers by working as physical separators. This general method, with structural diversity, is more conducive to extend the family of crystalline CTFs and optimize crystalline CTFs with high photocatalytic activity.